J|A|C|S
ARTICLES
Published on Web 04/20/2006

High-Quality Sodium Rare-Earth Fluoride Nanocrystals: Controlled Synthesis and Optical Properties

Hao-Xin Mai,[†] Ya-Wen Zhang,*[,†] Rui Si,[†] Zheng-Guang Yan,[†] Ling-dong Sun,[†] Li-Ping You,[‡] and Chun-Hua Yan*[,†]

Contribution from the Beijing National Laboratory for Molecular Sciences, State Key Lab of Rare Earth Materials Chemistry and Applications & PKU-HKU Joint Lab in Rare Earth Materials and Bioinorganic Chemistry, Peking University, Beijing 100871, China, Electron Microscopy Laboratory, Peking University, Beijing 100871, China

Received January 11, 2006; Revised Manuscript Received March 16, 2006; E-mail: yan@pku.edu.cn

Abstract: We report a general synthesis of high-quality cubic (α-phase) and hexagonal (β-phase) $NaREF_4$ (RE: Pr to Lu, Y) nanocrystals (nanopolyhedra, nanorods, nanoplates, and nanospheres) and $NaYF_4$:Yb,Er/Tm nanocrystals (nanopolyhedra and nanoplates) via the co-thermolysis of $Na(CF_3COO)$ and $RE(CF_3COO)_3$ in oleic acid/oleylamine/1-octadecene. By tuning the ratio of Na/RE, solvent composition, reaction temperature and time, we can manipulate phase, shape, and size of the nanocrystals. On the basis of its $\alpha \rightarrow \beta$ phase transition behavior, along the rare-earth series, $NaREF_4$ can be divided into three groups (I: Pr and Nd; II: Sm to Tb; III: Dy to Lu, Y). The whole controlled-synthesis mechanism can be explained from the point of view of free energy. Photoluminescent measurements indicate that the value of I_{610}/I_{590} and the overall emission intensity of the $NaEuF_4$ nanocrystals are highly correlative with the symmetries of the Eu^{3+} ions in both the lattice and the surface.

Introduction

Chemical, physical, and materials studies on the nanometer scale have experienced an enormous development since the 1990s and have led to the appearance of the new interdisciplinary fields of "nanoscience and nanotechnology".[1] In these fields, high-quality dispersible inorganic nanocrystals allow the investigation of their size-/shape-dependent properties and promise many applications in optics, catalysis, biosensing, and data storage,[1b,c,2] and are of fundamental and technological importance. Precise control of the size and shape allows manipulation of the properties of the nanocrystals as desired.[2,3] In addition, phase control is crucially important, as the properties of the materials are determined first by their phase. Moreover, the phases of the crystalline seeds can induce different growth kinetics (isotropically or anisotropically) of the nanocrystals,[3] and nanomaterials with different shapes can be obtained. Developing new synthetic pathways toward such nanomaterials (e.g., metals and metal alloys, II−VI and III−V group semiconductors, and metal oxides), investigating their material properties, and uncovering the underlying size/shape/phase control principles are thus of great interest.[1c,2c,4] Up to the present, the relatively successful synthetic methods are the organometallic approach and its alternatives.[1c,2c,4] With these methods, it still remains an open challenge to identify a suitable synthetic route and the associated synthetic parameters for growing high-quality (monodisperse, single-crystalline, well-shaped, and phase-pure) products of a given inorganic material. Recent studies have revealed the keys to a successful synthesis lie in the following three aspects: (i) a careful choice of the precursors (kinds of various precursors and feeding form either in single source or multisource), (ii) a fine-tuning of the coordinating behavior of the solvents using coordinating and noncoordinating surfactants, and (iii) a well-maintained balance between nucleation and growth stages.[3−5]

Dispersible nanocrystals of rare-earth compounds, such as oxides,[6] phosphates,[7] fluorides,[8] vanadates,[9] and sulfides,[10] have become a new focus of research, due to their unique properties

[†] State Key Lab of Rare Earth, Peking University.
[‡] Electron Microscopy Laboratory, Peking University.

(1) (a) Iijima, S. *Nature* **1991**, *354*, 56. (b) Alivisatos, A. P. *Science* **1996**, *271*, 933. (c) Murray, C. B.; Norris, D. J.; Bawendi, M. G. *J. Am. Chem. Soc.* **1993**, *115*, 8706. (d) Hu, J. T.; Odom, T. W.; Lieber, C. M. *Acc. Chem. Res.* **1999**, *32*, 435. (e) Xia, Y. N.; Yang, P. D.; Sun, Y. G.; Wu, Y. Y.; Mayers, B.; Gates, B.; Yin, Y. D.; Kim, F.; Yan, H. Q. *Adv. Mater.* **2003,** *15*, 353.
(2) (a) Ahmadi, T. S.; Wang, Z. L.; Green, T. C.; Henglein, A.; El-Sayed, M. A. *Science* **1996**, *272*, 1924. (b) Bruchez, M.; Moronne, M.; Gin, P.; Weiss, S.; Alivisatos, A. P. *Science* **1998**, *281*, 2013. (c) Sun, S. H.; Murray, C. B.; Weller, D.; Folks, L.; Moser, A. *Science* **2000**, *287*, 1989.
(3) (a) Yin, Y. D.; Alivisatos, A. P. *Nature* **2005**, 437, 664. (b) Jun, Y. W.; Lee, J. H.; Choi, J. S.; Cheon, J. *J. Phys. Chem. B* **2005**, 109, 14795.
(4) (a) Dinega, D. P.; Bawendi, M. G. *Angew. Chem., Int. Ed.* **1999**, *38*, 1788. (b) Shevchenko, E. V.; Talapin, D. V.; Schnablegger, H.; Kornowski, A.; Festin, O.; Svedlindh, P.; Haase, M.; Weller, H. *J. Am. Chem. Soc.* **2003,** *125*, 9090. (c) Park, J.; Lee, E.; Hwang, N. M.; Kang, M.; Kim, S. C.; Hwang, Y.; Park, J. G.; Noh, H. J.; Kim, J. Y.; Park, J. H.; Hyeon, T. *Angew. Chem., Int. Ed.* **2005**, *44*, 2872. (d) Seo, W. S.; Shim, J. H.; Oh, S. J.; Lee, E. K.; Hur, N. H.; Park, J. T. *J. Am. Chem. Soc.* **2005**, *127*, 6188. (e) Chen, Y. F.; Kim, M.; Lian, G. D.; Johnson, M. B.; Peng, X. G. *J. Am. Chem. Soc.* **2005**, *127*, 13331. (f) Trindade, T.; O'Brien, P.; Zhang, X. M. *Chem. Mater.* **1997**, *9*, 523. (g) Yuhas, B. D.; Zitoun, D. O.; Pauzauskie, P. J.; He, R.; Yang, P. D. *Angew. Chem., Int. Ed.* **2006**, *45*, 420.
(5) (a) Peng, Z. A.; Peng, X. G. *J. Am. Chem. Soc.* **2001**, *123*, 1389. (b) Peng, Z. A.; Peng, X. G. *J. Am. Chem. Soc.* **2002**, *124*, 3343.
(6) (a) Cao, Y. C. *J. Am. Chem. Soc.* **2004**, *126*, 7456. (b) Si, R.; Zhang, Y. W.; You, L. P.; Yan, C. H. *Angew. Chem., Int. Ed.* **2005**, *44*, 3256. (c) Yu, T.; Joo, J.; Park, Y. I.; Hyeon, T. *Angew. Chem., Int. Ed.* **2005**, *44*, 7411.
(7) Kompe, K.; Borchert, H.; Storz, J.; Lobo, A.; Adam, S.; Moller, T.; Haase, M. *Angew. Chem., Int. Ed.* **2003**, *42*, 5513.

 10.1021/ja060212h CCC: $33.50

arising from the 4f electron configuration and the potential applications in ultraviolet absorbants, solid-state lasers, optical amplifiers, lighting and displays, and biolabels. Among them, rare-earth fluoride nanocrystals have attracted particular interest due to their potential uses in optics, optoelectronics, microelectronics, and tribology.[11] As an important category of rare-earth fluoride compounds, $AREF_4$ (A = alkali; RE = rare earth), with unique luminescent, ferromagnetic, insulating/magnetic, and piezoelectric properties has drawn more attention because of the applications in solid-state lasers, three-dimensional flat-panel displays, and low-intensity IR imaging.[12] Particularly, recent advances revealed that their nanosized up-conversion (UC) phosphors can serve as white-light sources and sensitive bioprobes.[11c,12a,b,h] As known, hexagonal $NaYF_4$ is the most efficient host material for green and blue up-conversion phosphors until now, which exhibits visible emission upon infrared (IR) excitation when doped with Yb^{3+} and Er^{3+}/Tm^{3+}.[13] However, how to avoid the detrimental effect of oxygen contamination, surface hydroxyl groups, and impurity phases is still a challenge to enhance the UC efficiency of the $NaYF_4$ phosphors.[13] Therefore, it is critically important to develop a new synthetic method to obtain high-quality $NaYF_4$:Yb,Er/Tm nanocrystals. There are some recent reports on the syntheses of 0D (dots)[12a−c] and 1D (rods[12b] and tubes[12g]) nanostructures of $AREF_4$ with limited wet chemical approaches involving modified coprecipitation,[12c] reversed micelle,[12c] and hydrothermal methods,[12b,c,g] whereas dispersible nanocrystals have rarely been prepared.[12a] Until now, all the developed synthetic methods available for $AREF_4$ nanocrystals are substantially based on the liquid precipitation reaction between soluble rare-earth salts and alkali fluorides.

In the present work, we demonstrate for the first time a general one-step synthesis of dispersible high-quality $NaREF_4$ (RE = Pr to Lu, Y), Yb^{3+}, and Er^{3+}/Tm^{3+} codoped $NaYF_4$ nanocrystals via the co-thermolysis of $Na(CF_3COO)$ and $RE(CF_3COO)_3$ precursors in the solvent of oleic acid/oleylamine/1-octadecene. In each precursor, both metal (either Na or RE) and fluorine elements are integrated in the same compound, which may provide a much better controlled-synthesis of fluoride nanocrystals than the liquid precipitation methods.[8b] The as-synthesized rare-earth fluoride nanocrystals have shown intriguing self-assembly capability and easily form the superlattice.[8b,d] Through controlling the nanocrystal growth kinetics in the combined solvent, phase-/size-/shape-controlled single-crystalline and monodisperse $NaREF_4$ nanopolyhedra, nanorods, nanoplates, and nanospheres were prepared (Tables S1, S2, and S3), among which, $NaEuF_4$ nanopolyhedra, nanorods, and nanospheres showed interesting photoluminescent (PL) properties.

Experimental Section

The synthesis was carried out using standard oxygen-free procedures and commercially available reagents. Rare-earth oxides, oleic acid (OA; 90%, Alpha), oleylamine (OM; >80%, Acros), 1-octadecene (ODE; >90%, Acros), trifluoroacetic acid (99%, Acros), $M(CF_3COO)$ (M = Na, K; >97%, Acros), absolute ethanol, chloroform, hexane, and toluene were used as received. $RE(CF_3COO)_3$ and $Li(CF_3COO)$ were prepared with the literature method.[14]

Synthesis of High-Quality α-$NaREF_4$ (RE = Pr to Lu, Y) and β-$NaREF_4$ (RE = Pr, Nd, Dy to Lu, Y) Nanocrystals. A typical procedure is as follow: to a three-necked flask of 40 mmol OA/OM/ODE (Tables S1 and S2) at room temperature were added given amounts of $Na(CF_3COO)$ and $RE(CF_3COO)_3$ (1 mmol). Then the slurry was heated to 100 °C to remove water and oxygen, with vigorous magnetic stirring under vacuum for 30 min in a temperature-controlled electromantle, and thus to form a transparent solution. The solution was then heated to a certain temperature in the range of 250−330 °C at a rate of 20 K min^{-1} and maintained at the given temperature for 15−45 min under an Ar atmosphere. When the reaction was completed, an excessive amount of ethanol was poured into the solution at room temperature. The resultant mixture was centrifugally separated, and the products were collected. The as-precipitated nanocrystals were washed several times with ethanol and dried in air at 70 °C overnight. The yields of all the obtained nanocrystals without any size selection were 60−70%. All of these as-prepared nanocrystals could be easily redispersed in various nonpolar organic solvents such as hexane, toluene, and chloroform.

Synthesis of High-Quality β-$NaREF_4$ (RE = Sm to Tb) Nanocrystals. The synthetic procedure was the same as that used to synthesize β-$NaREF_4$ (RE = Pr, Nd, Dy to Lu, Y) nanocrystals, except that quantitative $Na(CF_3COO)$ and the as-prepared α-$NaREF_4$ (RE = Sm, Eu, Gd, or Tb) nanocrystals were taken as the precursors and were added into a mixture of 40 mmol OA/ODE (Table S3) in a three-necked flask at room temperature.

Synthesis of High-Quality α-$NaYF_4$:20%Yb,2%Er and α-$NaYF_4$:30%Yb,0.5%Tm Nanocrystals. The synthetic procedure was the same as that used to synthesize α-$NaYF_4$ nanocrystals, except that 1 mmol $Na(CF_3COO)$ and stoichiometric amounts of $Y(CF_3COO)_3$, $Yb(CF_3COO)_3$, and $Er(CF_3COO)_3/Tm(CF_3COO)_3$) were taken as the precursors and were added into a mixture of OA (10 mmol), OM (10 mmol), and ODE (20 mmol) in a three-necked flask at room temperature.

Synthesis of High-Quality β-$NaYF_4$:20%Yb,2%Er and β-$NaYF_4$:30%Yb,0.5%Tm Nanocrystals. The synthetic procedure was the same as that used to synthesize β-$NaYF_4$ nanocrystals, except that 2.5 mmol $Na(CF_3COO)$ and stoichiometric amounts of $Y(CF_3COO)_3$, $Yb(CF_3COO)_3$, and $Er(CF_3COO)_3/Tm(CF_3COO)_3$ were taken as the precursors and were added into a mixture of OA (20 mmol) and ODE (20 mmol) in a three-necked flask at room temperature.

Instrumentation. Powder X-ray diffraction (XRD) patterns of the dried powders were recorded on a Rigaku D/MAX-2000 diffractometer (Japan) with a slit of 1/2° at a scanning rate of 2° min^{-1}, using Cu Kα radiation (λ = 1.5406 Å). The lattice parameters were calculated with the least-squares method. Samples for transmission electron microscopy (TEM) analysis were prepared by drying a nanocrystal dispersion in hexane/toluene (v/v = 1:1) on amorphous carbon-coated copper grids.

(8) (a) Stouwdam, J. W.; van Veggel, F. C. J. M. *Nano Lett.* **2002**, *2*, 733. (b) Zhang, Y. W.; Sun, X.; Si, R.; You, L. P.; Yan, C. H. *J. Am. Chem. Soc.* **2005**, *127*, 3260. (c) Sudarsan, V.; Sivakumar, S.; van Veggel, F. C. J. M.; Raudsepp, M. *Chem. Mater.* **2005**, *17*, 4736. (d) Shevchenko, E. V.; Talapin, D. V.; Kotov, N. A.; O'Brien, S.; Murray, C. B. *Nature* **2006**, *439*, 55.
(9) Riwotzki, K.; Haase, M. *J. Phys. Chem. B* **1998**, *102*, 10129.
(10) Mirkovic, T.; Hines, M. A.; Nair, P. S.; Scholes, G. D. *Chem. Mater.* **2005**, *17*, 3451.
(11) (a) Zhou, J. F.; Wu, Z. S.; Zhang, Z. J.; Liu, W. M.; Dang, H. X. *Wear* **2001**, *249*, 333. (b) Wang, X.; Li, Y. D. *Angew. Chem., Int. Ed.* **2003**, *42*, 3497. (c) Sivakumar, S.; van Veggel, F. C. J. M.; Raudsepp, M. *J. Am. Soc. Chem.* **2005**, *127*, 12464.
(12) (a) Heer, S.; Kompe, K.; Gudel, H. U.; Haase, M. *Adv. Mater.* **2004**, *16*, 2102. (b) Zeng, J. H.; Su, J.; Li, Z. H.; Yan, R. X.; Li, Y. D.; *Adv. Mater.* **2005**, *17*, 2119. (c) Karbowiak, M.; Mech, A.; Bednarkiewicz, A.; Strek, W.; Kepinski, L. *J. Phys. Chem. Solids* **2005**, *66*, 1008. (d) Cooke, A. H.; Jones, D. A.; Silva, J. F. A.; Wells, M. R. *J. Phys. C* **1975**, *8*, 4083. (e) Ghosh, S.; Rosenbaum, T. F.; Aeppli, G.; Coppersmith, S. N. *Nature* **2003**, *425*, 48. (f) Choi, B.; Moon, B.; Seo, H.; Jeong, J.; Lee, H.; Seo, W. *Mater. Design* **2000**, *21*, 567. (g) Liang, L. F.; Xu, H. F.; Su, Q.; Konishi, H.; Jiang, Y. B.; Wu, M. M.; Wang, Y. F.; Xia, D. Y. *Inorg. Chem.* **2004**, *43*, 1594. (h) Yi, G. S.; Lu, H. C.; Zhao, S. Y.; Yue, G.; Yang, W. J.; Chen, D. P.; Guo, L. H. *Nano Lett.* **2004**, *4*, 2191.
(13) (a) Menyuk, N.; Dwight, K.; Pierce, J. W. *Appl. Phys. Lett.* **1972**, *21*, 159. (b) Suyver, J. F.; Aebischer, A.; Biner, D.; Gerner, P.; Grimm, J.; Heer, S.; Kramer, K. W.; Reinhard, C.; Gudel, H. U. *Opt. Mater.* **2005**, *27*, 1111. (c) Kramer, K. W.; Biner, D.; Frei, G.; Gudel, H. U.; Hehlen, M. P.; Luthi, S. R. *Chem. Mater.* **2004**, *16*, 1244. (d) Liang, L. F.; Wu, H.; Hu, H. L.; Wu, M. M.; Su, Q. *J. Alloy Compd.* **2004**, *368*, 94.
(14) Roberts, J. E. *J. Am. Chem. Soc.* **1961**, *83*, 1087.

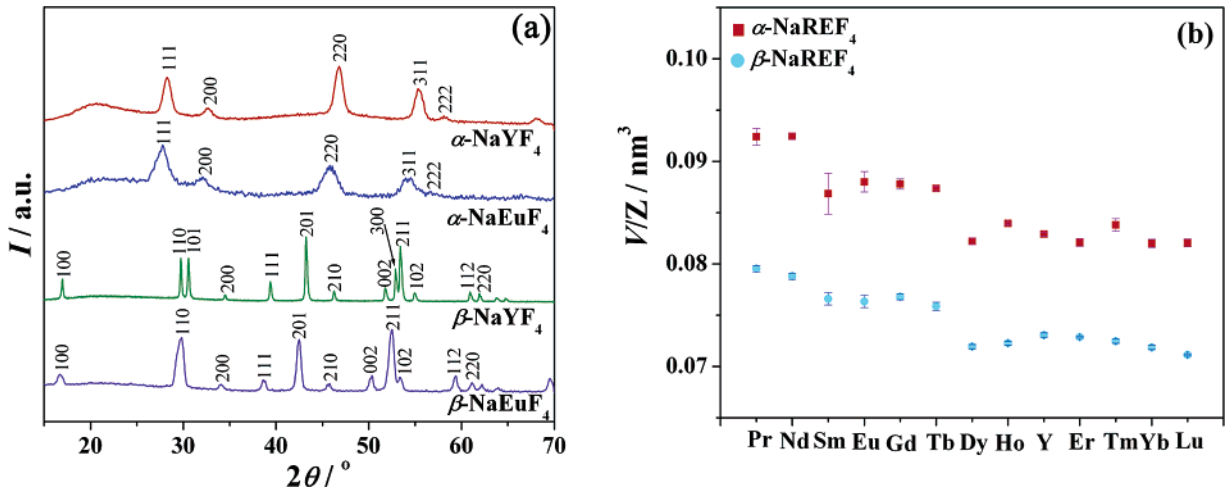

Figure 1. (a) XRD patterns of α-$NaYF_4$, α-$NaEuF_4$, β-$NaYF_4$, and β-$NaEuF_4$ nanocrystals. (b) Plots of the measured lattice volume over the number of $NaREF_4$ molecules (Z) in one unit cell against the rare-earth series.

Particle sizes and shapes were examined by a TEM (200CX, JEOL, Japan) operated at 160 kV. High-resolution TEM (HRTEM) characterization was performed with a Philips Tecnai F30 FEG-TEM operated at 300 kV. Room-temperature fluorescence spectra were recorded on a Hitachi F-4500 spectrophotometer equipped with a 150 W Xe-arc lamp at a fixed band-pass of 0.2 nm with the same instrument parameters (2.5 nm for excitation split, 2.5 nm for emission split and 700 V for PMT voltage), with the samples of α-$NaEuF_4$ (or β-$NaEuF_4$) nanocrystals dispersed in hexane/toluene (v/v = 1:1) at a concentration of 0.1 mol L^{-1}.

Results and Discussion

1. Characterization of α-$NaREF_4$ and β-$NaREF_4$ Nanocrystals. The XRD patterns shown in Figures 1a and S1 reveal that α-$NaREF_4$ and β-$NaREF_4$ (RE = Pr to Lu, Y) were formed. All the diffraction peaks for α-$NaREF_4$ shown in Figures 1a and S1a are characteristic of a pure cubic phase (space group: $Fm\bar{3}m$). The calculated lattice constants are: a = 5.493(2) Å for α-$NaYF_4$,[12a,15] and a = 5.603(1) Å for α-$NaEuF_4$ (JCPDS: 27-691). All of the XRD peaks for each β-$NaREF_4$ sample in Figures 1a and S1b can be indexed to a pure hexagonal phase (space group: P-6 or $P6_3/m$), in good agreement with the JCPDS data. The calculated lattice constants are: a = 5.991(5) Å and c = 3.526(4) Å for β-$NaYF_4$,[15] and a = 6.04(2) Å and c = 3.62(1) Å for β-$NaEuF_4$ (JCPDS: 28-1085). The broadening of the reflections ascribed to α-$NaEuF_4$ and α-$NaYF_4$ distinctly indicated their nanocrystalline nature, and the sharper reflections for β-$NaEuF_4$ and β-$NaYF_4$ implied their larger sizes compared with those of the former two samples. As shown in Figure 1b, the plots of unit cell volume per $NaREF_4$ molecule along the rare-earth series are in agreement with the lanthanide contraction. The atomic ratios of metals in the nanocrystals were determined by energy-dispersive X-ray analysis (EDAX), confirming the formation of stoichiometric $NaREF_4$ (Figure S2).

The TEM and HRTEM images shown in Figures 2, 3, S3, and S4 demonstrate that all of the as-obtained nanocrystals are of single-crystalline nature and display high crystallite size uniformity. Panels a−d of Figure 2 show the TEM images of the as-obtained α-$NaNdF_4$, α-$NaEuF_4$, α-$NaYF_4$, and α-$NaYbF_4$, respectively. All α-phase products are of polyhedron shape and have a uniform size of 5.9 nm for α-$NaNdF_4$, 6.3 nm for

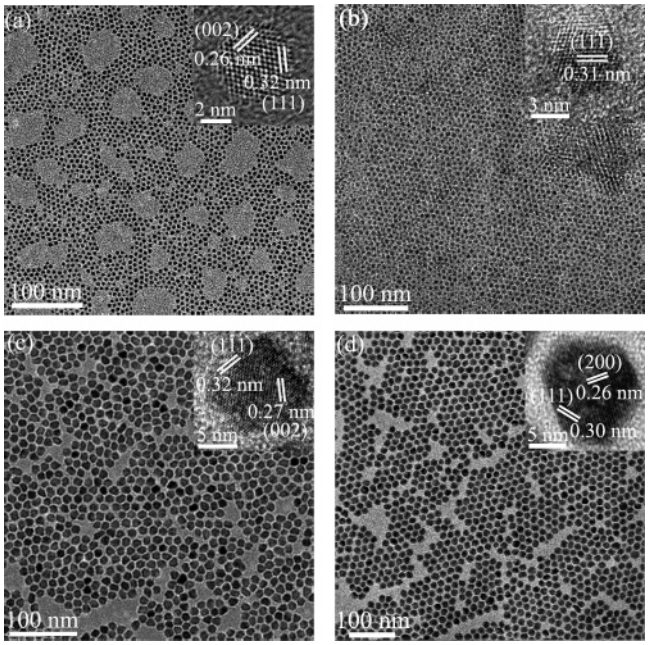

Figure 2. TEM and HRTEM (inset) images of α-$NaNdF_4$ (a), α-$NaEuF_4$ (b), α-$NaYF_4$ (c), and α-$NaYbF_4$ (d) nanopolyhedra.

α-$NaEuF_4$, 12.2 nm for α-$NaYF_4$, and 15.9 nm for α-$NaYbF_4$. The insets in Figure 2 show that α-$NaNdF_4$, α-$NaEuF_4$, α-$NaYF_4$, and α-$NaYbF_4$ are of truncated octahedron shape, enclosed by the (111) and (002) planes.[16] From Figures 2 and S3, it is also noted that the as-obtained α-$NaREF_4$ nanocrystals are well-separated and exhibit a remarkable 2D-ordered arrangement, indicative of the presence of capping ligands on the surfaces of the nanocrystals, which was confirmed by ^{1}H NMR measurements (Figure S5).

Figure 3a reveals that all of the 26.6 nm × 47.6 nm (diameter from corner to corner × height) β-$NaYF_4$ nanorods redispersed in toluene/hexane (v/v = 1:1) stand on the TEM grids via the side faces. When increasing the polarity of the dispersant by the addition of ethanol (toluene/hexane/ethanol = 1:1:0.48), some nanorods stand on the TEM grids on their bottom faces, showing a hexagonal cross-section (Figure 3b). As disclosed by HRTEM images, the β-$NaYF_4$ nanorods show a preferred

(15) Thoma, R. E.; Insley, H.; Hebert, G. M. *Inorg. Chem.* **1966**, *5*, 1222.

(16) Wang, Z. L. *J. Phys Chem. B* **2000**, *104*, 1153.

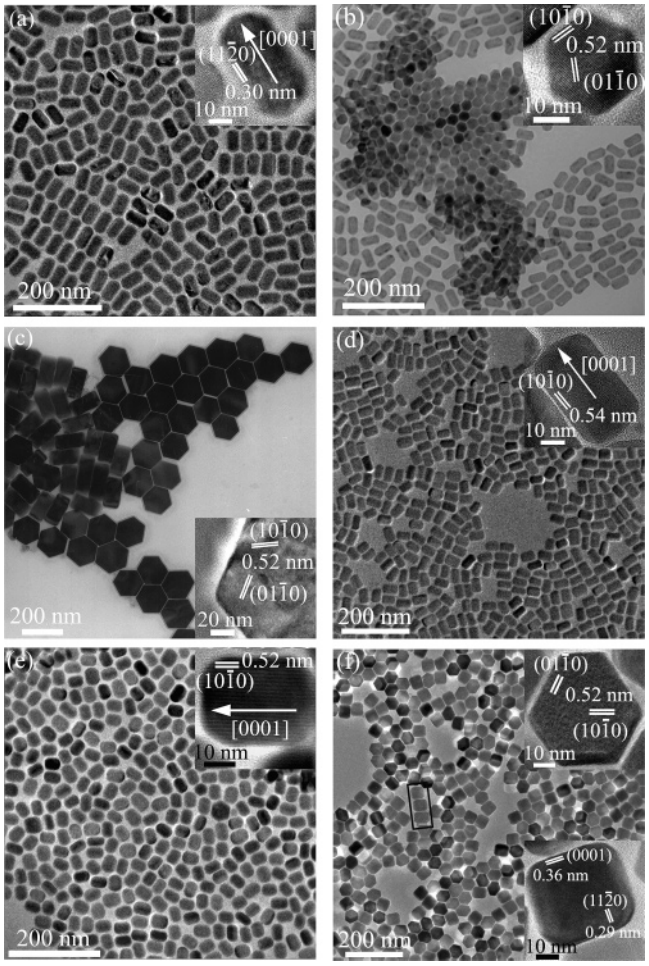

Figure 3. TEM and HRTEM (inset) images of β-$NaYF_4$ nanorods redispersed in toluene/hexane (1:1) (a) and in toluene/hexane/ethanol (1:1:0.48) (b), of β-$NaYF_4$ nanoplates (c), of β-$NaNdF_4$ nanorods (d), and of β-$NaEuF_4$ nanorods (e). TEM and HRTEM (inset, upper: lying flat on the face; lower: standing on the side face from the highlighted square) images of β-$NaHoF_4$ hexagonal plates (f).

growth direction along [0001] and are enclosed by {10−10} and {0001} facets (insets in a and b of Figure 3). When increasing the ratio of Na:Y from 1.8 to 2.1, we obtained 155 nm × 76 nm β-$NaYF_4$ hexagonal nanoplates (Figure 3c), standing on the TEM grids on either the bottom face or the side face. The HRTEM images (insets in Figures 3c and S6) show that the nanoplates are enclosed by {10−10} and {0001} facets. Panels d and e of Figure 3 reveal the formation of 26.1 nm × 43.8 nm β-$NaNdF_4$ and 24.6 nm × 35.7 nm β-$NaEuF_4$ nanorods, respectively, with a 1D nanostructure with a preferred growth direction along [0001] (insets in d and e of Figure 3). Figure 3f shows the formation of β-$NaHoF_4$ hexagonal plates (either lying flat on the bottom face or standing on the side face) in the size of 52.7 nm × 43.2 nm. The insets in Figure 3f indicate that β-$NaHoF_4$ hexagonal nanoplates are enclosed by {10−10} and {0001} facets.

2. Formation Conditions of Pure α-$NaREF_4$ or β-$NaREF_4$. $NaREF_4$ exists in two polymorphs at ambient pressure: cubic α-phase (metastable high-temperature phase) and hexagonal β-phase (thermodynamically stable low-temperature phase).[15] In the structure of α-$NaREF_4$, Na^+ and RE^{3+} cations are randomly distributed in the cationic sublattice, while in β-$NaREF_4$ the cation sites are of three types: a one-fold site occupied by RE^{3+}, a one-fold site occupied randomly by $1/2Na^+$ and $1/2RE^{3+}$, and a two-fold site occupied randomly by Na^+ and vacancies. Thus, the transformation from α-$NaREF_4$ into β-$NaREF_4$ is of a disorder-to-order character with respect to cations (Figure S7).[15] In this work, the phase-controlled syntheses of high-quality α-$NaREF_4$ and β-$NaREF_4$ nanocrystals have been carefully conducted. The synthetic parameters including the ratios of Na/RE and OA/OM/ODE, reaction time, and temperature were demonstrated to play key roles (Table S4). The coordination behavior of the combined solvents was tuned by varying the relative content of the coordinating solvent (oleic acid/oleylamine) to noncoordinating solvent (1-octadecene).

As known, for bulk $NaREF_4$ along the rare-earth series, the α-phase is unstable below temperatures varying from 800 °C (for α-$NaPrF_4$) to 530 °C (for α-$NaLuF_4$). On cooling, they would transform into a variety of products, depending on the compositions of the decomposing phases.[15] In our work, however, nanosized α-$NaREF_4$ (RE = Pr to Lu, Y; except La and Ce) was stable even at room temperature. It was shown that LaF_3 or CeF_3 was preferred to segregate along with NaF, instead of forming $NaLaF_4$ or $NaCeF_4$. Pure α-$NaREF_4$ could be obtained at a low temperature and a low ratio of Na/RE in OA/OM/ODE with a relatively short reaction time, while β-$NaREF_4$ was formed under the reverse conditions. On the basis of its $\alpha \rightarrow \beta$ phase transition behavior, $NaREF_4$ along the rare-earth series can be divided into three groups (I: Pr and Nd; II: Sm to Tb; III: Dy to Lu, Y). For the OA/ODE reaction system, β-$NaREF_4$ in groups I and III was formed only under drastic conditions (high Na/RE, 330 °C, and long reaction time), while those in group II could be formed even under mild conditions, possibly due to the best-matching ion radius of Na^+ to RE^{3+}.[15] For group I, REF_3 was preferred to form, whereas α-$NaREF_4$ was preferred for group III. With the addition of OM into OA/ODE, α-$NaREF_4$ became more stable and was thus preferred to form (Table S4 and Figure S8).

3. Synthesis of High-Quality α-$NaREF_4$ Nanocrystals. On the basis of the above phase-control studies along the rare-earth series, high-purity α-$NaREF_4$ and β-$NaREF_4$ nanocrystals can be selectively synthesized with choosing appropriate synthetic parameters. As is well-known, sustaining a balance between nucleation and growth stages is prerequisite for the synthesis of monodisperse nanocrystals.[3,4−6] For the crystalline seeds with an isotropic unit cell structure (e.g., cubic), they often experience an isotropic growth, which results in 0D-nanostructures.[3,4−6] This is also the case in the present work, in which α-$NaREF_4$ nanocrystals exhibited a typical 0D-growth shape (nanopolyhedra). To obtain high-quality products, optimal synthetic parameters were screened so as to achieve the proper balance between the nucleation and growth stages.

We first investigated the nucleation and growth stages of α-$NaREF_4$ nanocrystals. As the solution containing both Na(CF_3COO) and RE(CF_3COO)$_3$ was rapidly heated to around 250 °C under an Ar atmosphere, some tiny gas bubbles emitted from the reaction system promptly, which implied an instant co-decomposition of the precursors and a simultaneous formation of $NaREF_4$ nuclei.[8b,14] Determined with a gas chromatograph/mass spectrometer, the major components of the gas bubbles were CO_2 and fluorinated/oxyfluorinated carbon species. When the Na/RE ratio, reaction temperature, and time were fixed, the solvent composition was found to greatly affect the growth of

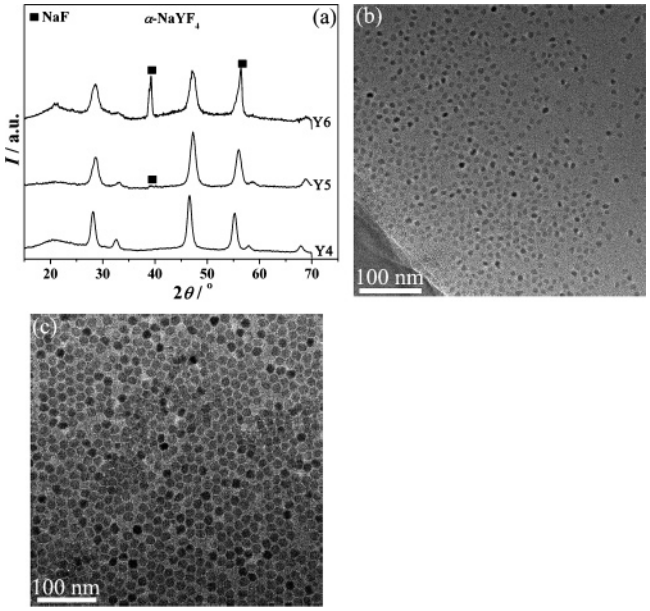

Figure 4. XRD patterns (a) of some α-$NaYF_4$ samples (**Y4**: 1 mmol Na(CF_3COO) and 1 mmol $Y(CF_3COO)_3$, OA/OM/ODE = 1.5:0.5:2, 250 °C, 45 min; **Y5**: 1 mmol Na(CF_3COO) and 1 mmol $Y(CF_3COO)_3$, OA/OM/ODE = 0.5:1.5:2, 250 °C, 45 min; **Y6**: 1 mmol Na(CF_3COO) and 1 mmol $Y(CF_3COO)_3$, OM/ODE = 1:1, 250 °C, 45 min). TEM images of 9.2 nm (b) and 15.9 nm (c) α-$NaYF_4$ nanopolyhedra.

high-quality nanocrystals. Taking α-$NaYF_4$ as an example, the presence of too much oleic acid ligands yielded highly crystallized but severely agglomerated nanocrystals, implying that the growth of the α-$NaYF_4$ nanocrystals became drastic with the addition of more OA (Figures 4a and S9a). In the presence of too many OM ligands, it produced dispersed but ill-shaped nanocrystals with few NaF impurities (Figures 4a and S9b). It seems that the addition of excess OM might hinder the growth of α-$NaYF_4$, and thus more NaF segregated with increasing the value of OM/OA (Figure 4a). Therefore, high-quality α-$NaYF_4$ nanopolyhedra were obtained at an optimized OA/OM/ODE ratio of 1:1:2 (Figure 2c), due to a well-maintained balance between nucleation and growth stages during the synthesis under this condition.[4−6]

The growth kinetics of the other high-purity α-$NaREF_4$ nanocrystals was investigated and found to resemble that of α-$NaYF_4$ nanocrystals. The size of α-$NaYF_4$ nanopolyhedra can be tuned through changing the reaction temperature. Under Na/Y = 1:1, OA/OM/ODE = 1:1:2 and 45 min, lowering the temperature from 250 to 240 °C decreased the size of α-$NaYF_4$ nanopolyhedra from 12.8 to 9.2 nm with a lower yield (30%) (Figure 4b), whereas increasing the temperature to 270 °C for 30 min, 15.9 nm α-$NaYF_4$ nanopolyhedra were obtained (Figure 4c). Under the reaction temperature higher than 270 °C, the size of the nanopolyhedra increased further, but their size distribution became markedly broad. The growth of high-purity α-$NaEuF_4$ nanocrystals was similar to that of α-$NaYF_4$ ones (Figures 2b and S9c,d). For α-$NaNdF_4$, only 5.9 nm nanopolyhedra were obtained under 290 °C for 30 min (Figure 2a). Lowering the temperature below 290 °C yielded fewer products, while increasing temperature might lead to the α → β phase transition, which suggested that the formation region for high-purity α-$NaNdF_4$ nanocrystals was quite narrow.

4. Synthesis of High-Quality β-$NaREF_4$ Nanocrystals. In general, anisotropic structures (e.g., hexagonal) of the seeds can induce anisotropic growth along their crystallographically reactive directions; thus, anisotropic shapes of nanocrystals are expected.[3−6] For β-$NaREF_4$ in our case, both hexagonal nanorods and nanoplates were obtained (Figure 3). It was noted that rodlike nanocrystals were thermodynamically favored for groups I (Pr and Nd) and II (Sm to Tb), whereas platelike nanocrystals were favored for group III (Dy to Lu, Y). In this part, we tried to reveal the growth process of high-quality β-$NaREF_4$ nanocrystals on the basis of the above phase control studies and the α → β phase transition modes identified in the following.

Group I (Pr and Nd). The growth conditions for β-$NaREF_4$ nanocrystals for group I were different from those for other groups, as REF_3 rather than α-$NaREF_4$ was preferably formed in the synthetic process. Figure 5 disclosed the growth process of β-$NaNdF_4$ nanorods. At the very beginning (as soon as the reaction temperature was promoted to 330 °C), NdF_3 and NaF were formed (Figure 5a), and the nanoparticulate products were of irregular shape and were less uniform in size (Figure S10a). After 15 min of reaction, NaF and NdF_3 were partially consumed, and a small amount of β-$NaNdF_4$ was formed (Figure 5a). With prolonging the reaction time to 25 min, NaF and NdF_3 were consumed completely, and pure β-$NaNdF_4$ was formed, indicated with the XRD patterns in Figure 5a. Both irregular nanocrystals and well-shaped nanorods of β-$NaNdF_4$ were found

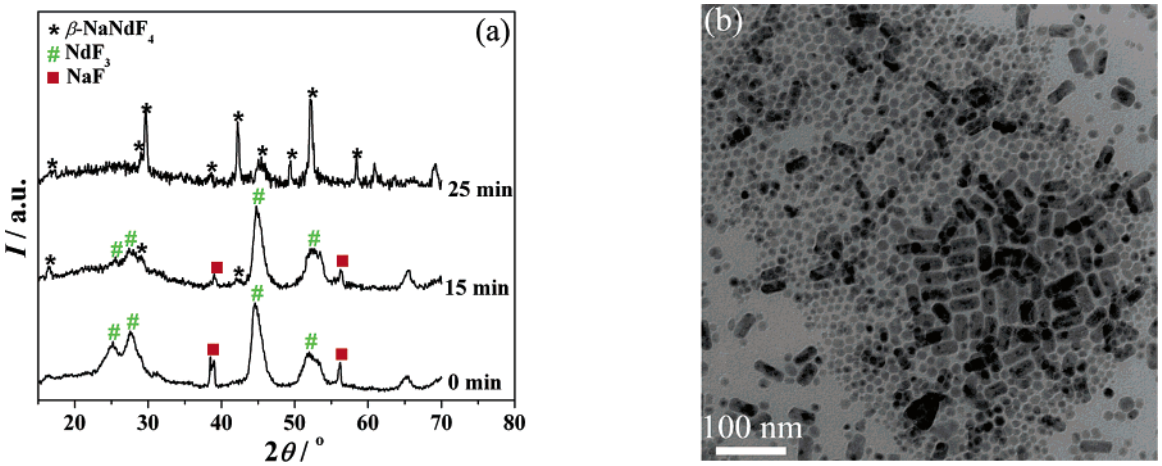

Figure 5. (a) XRD patterns of the products obtained under Na/Nd = 1.6:1 in OA/ODE (1:1) at 330 °C for 0−25 min. (b) TEM image of the product obtained under Na/Nd = 1.6:1 in OA/ODE (1:1) at 330 °C for 25 min.

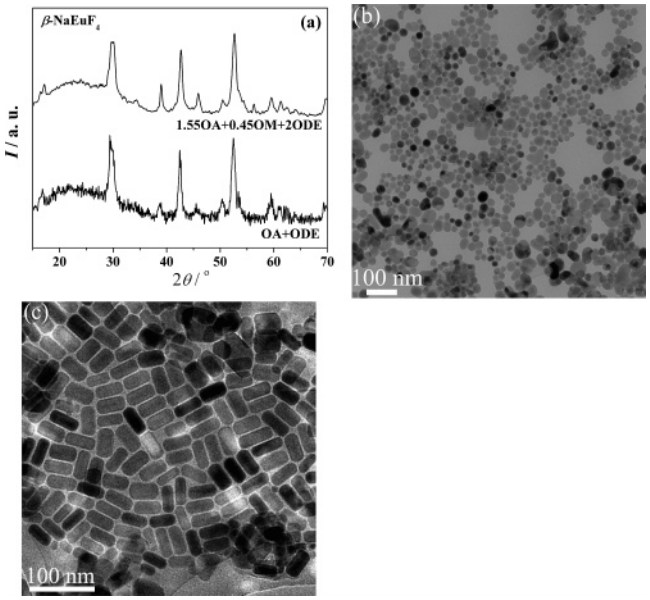

Figure 6. (a) XRD patterns of the products obtained under Na/Eu = 1.7:1 at 330 °C for 0 min in OA/OM/ODE. TEM images of the products: (b) OA/ODE (1:1) and (c) OA/OM/ODE (1.55:0.45:2) for 15 min.

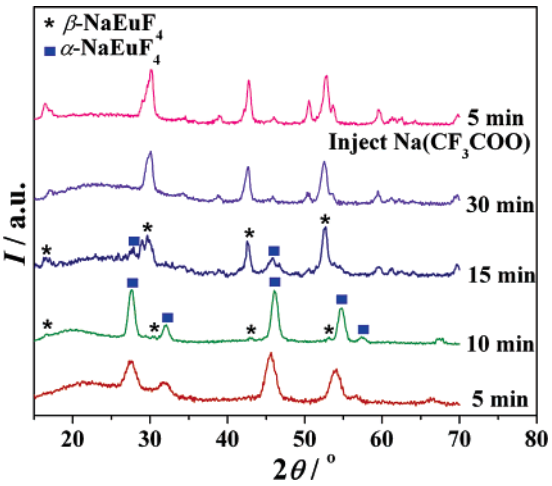

Figure 7. XRD patterns of the products obtained under 330 °C in OA/ODE (1:1) for 5−35 min (precursor: 1 mmol α-$NaEuF_4$ nanopolyhedra and 0.1 mmol $Na(CF_3COO)$; injection: 0.9 mmol $Na(CF_3COO)$ dissolved in 1 mL of OA/ODE after the 30 min reaction).

(Figure 5b). Uniform β-$NaNdF_4$ nanorods in the size of 26.1 nm × 43.8 nm were obtained with prolonging further the reaction time (Figure 3d). When the reaction time was extended to 1 h, β-$NaNdF_4$ nanorods grew a little larger with a nearly unchanged aspect ratio, but partial agglomeration occurred. It is suggested that the formation of the uniform β-$NaNdF_4$ nanorods underwent an Ostwald-ripening process, in which the irregular particles dissolved and the rodlike particles grew simultaneously (Figures 5 and S10a).[5] Moreover, when 1 mmol uniform α- $NaNdF_4$ nanopolyhedra was taken as the precursors dispersed in OA/ODE (1:1) for a reaction under 330 °C for 30 min, α- $NaNdF_4$ was transformed into NdF_3 and β-$NaNdF_4$ (Table S4). Then, 1 mmol $Na(CF_3COO)$ dissolved in 1 mL of OA/ODE was injected into the reaction system. After 30 min, uniform 26.3 nm × 60.6 nm β-$NaNdF_4$ nanorods were obtained (Figure S10b). As a result, we concluded that the rod might be the thermodynamically stable shape for β-$NaNdF_4$ due to the fact that its formation is independent of the reaction route we selected.

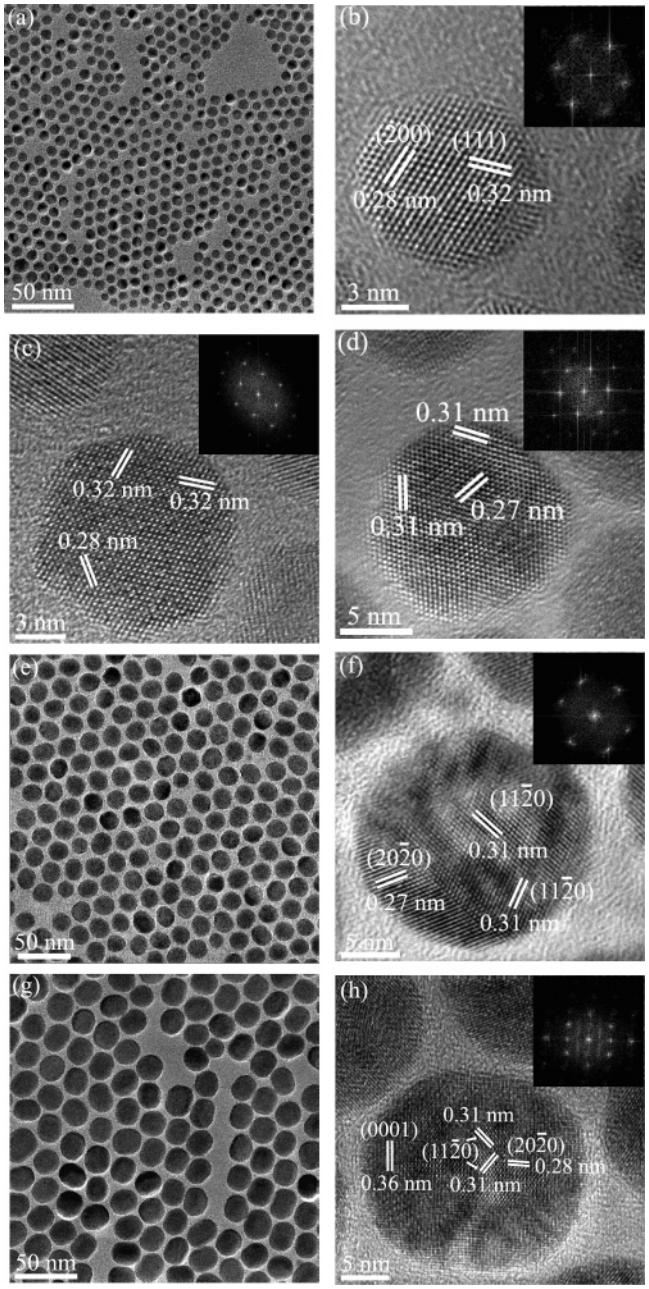

Figure 8. TEM images of the $NaEuF_4$ products: 5 min (a) and 30 min (e). HRTEM images with FFT analysis (inset) of the $NaEuF_4$ products: 5 min (b), 10 min (c), 15 min (d), 30 min (f). TEM (g) and HRTEM images (h) of the $NaEuF_4$ product obtained by a 5 min reaction after injecting 0.9 mmol $Na(CF_3COO)$ dissolved in 1 mL of OA/ODE into the solution reacted under 330 °C in OA/ODE (1:1) for 30 min (precursor: 1 mmol α-$NaEuF_4$ nanopolyhedra and 0.1 mmol $Na(CF_3COO)$).

Group II (Sm to Tb). As indicated above, β-$NaREF_4$ in group II was the easiest to form. This was further confirmed by the XRD patterns shown in Figure 6a, which reveals that pure β-$NaEuF_4$ was formed as soon as the reaction temperature reached 330 °C. No peaks ascribed to EuF_3 or α-$NaEuF_4$ can be found in Figure 6a, even in the case that a bit of OM was added into OA/ODE. In OA/ODE, only irregular and aggregated β-$NaEuF_4$ nanocrystals were obtained (Figure 6b), indicating that the Ostwald-ripening process occurred severely in this system.[5] Considering that the growth of β-$NaEuF_4$ was fast in OA/ODE, some OM were added to restrain the Ostwald-ripening process. Therefore, relatively regular rod-shaped nanocrystals

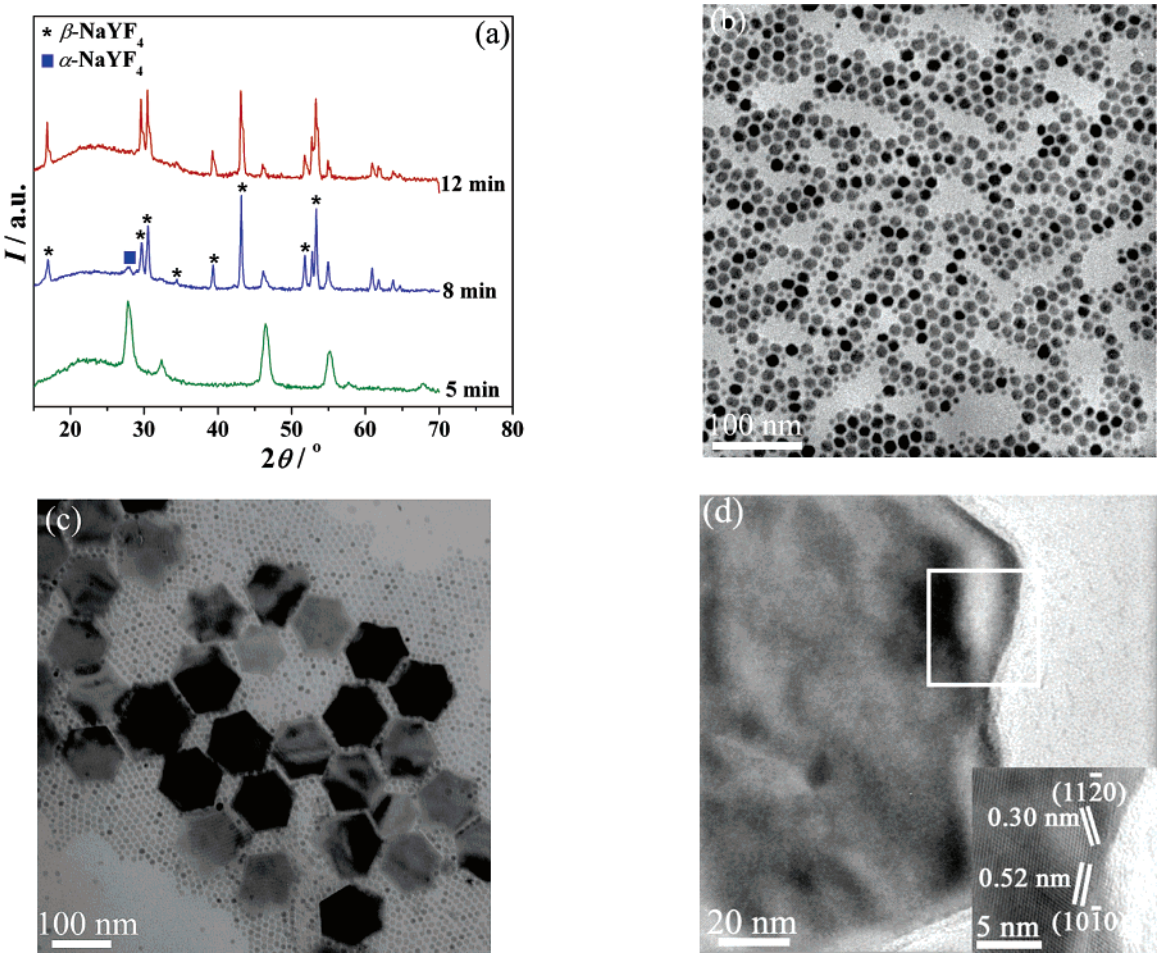

Figure 9. (a) XRD patterns of the products obtained under 330 °C in OA/ODE (1:1) for 5−12 min (precursor: 1 mmol α-$NaYF_4$ nanopolyhedra and 1 mmol $Na(CF_3COO)$). TEM images of the products: 5 min (b), 8 min (c), and 12 min (d) (inset: HRTEM image from the highlighted square).

were obtained (Figure 6c). In the OA/OM = 1.55:0.45 system, under the same reaction conditions, adding more OM decreased further the growth rate of β-$NaEuF_4$, and thus both nanorods and some nanocrystals with 1D growth tendency were found as OA/OM = 3:1.

To reveal the $\alpha \rightarrow \beta$ phase transition and growth kinetics of $NaEuF_4$ nanocrystals in detail, 1 mmol 6.3 nm α-$NaEuF_4$ nanopolyhedra and 0.1 mmol $Na(CF_3COO)$ were dissolved in OA/ODE for a reaction under 330 °C. With extending the reaction time, α-$NaEuF_4$ transformed gradually into β-$NaEuF_4$ (Figure 7) with the increase in particle size: 8.1 ± 0.5 nm at 5 min (pure α-$NaEuF_4$) (Figure 8a), 12.1 ± 0.7 nm at 10 min (α-$NaEuF_4$ along with a little β-$NaEuF_4$) (Figure S11a), 13.7 ± 1.2 nm at 15 min (α-$NaEuF_4$ and β-$NaEuF_4$) (Figure S11b), and 19.1 ± 0.9 nm at 30 min (pure β-$NaEuF_4$) (Figure 8e). From the HRTEM images, it was also noted that the lattice fringe patterns of all of these nanocrystals in every stage of the phase transition (Figure 8b−d,f) looked similar. For the pure α-$NaEuF_4$ nanopolyhedra, the interplanar spacing of 0.32 and 0.28 nm was indexed as (111) and (200) lattice fringes, respectively (Figure 8b), while for the pure β-$NaEuF_4$ nanospheres, the interplanar spacing of 0.31 and 0.27 nm was indexed as (11−20) and (20−20) lattice fringes, respectively (Figure 8f). Further prolonging the reaction time did not lead to the obvious size increase for the spherical particles but only caused the aggregation.

As discussed above, the $\alpha \rightarrow \beta$ phase transition process for $NaEuF_4$ nanocrystals can be concluded. The growth of $NaEuF_4$ nanocrystals was mild, and they kept a spherical shape at a low concentration (0.025 mol L^{-1}) of $Na(CF_3COO)$. Their sizes gradually increased from 8.1 to 19.1 nm through extending the reaction time from 5 to 30 min. It is also seen that differently sized $NaEuF_4$ nanocrystals were monodisperse during the whole process, due to size standard deviations of less than 10% at every stage, even they showed a relatively broader size distribution at the mix-phase stage (Figure S11e). Also considering the results obtained with XRD (Figure 7), there is a critical size for the transition from α-$NaEuF_4$ nanocrystals to β-$NaEuF_4$ ones. When the size of $NaEuF_4$ nanocrystals was less than 12 nm (Figure 8a), cubic $NaEuF_4$ was stable (Figure 7), whereas as the size exceeded 12 nm, $\alpha \rightarrow \beta$ phase transition occurred (Figures 7, S11a, and S11b) and the size for obtaining pure hexagonal $NaEuF_4$ might be 18−19 nm (Figures 7 and 8e). For this reason, it is possible that 12 nm was the critical size for the transition from α-$NaEuF_4$ to β-$NaEuF_4$. The $\alpha \rightarrow \beta$ phase transition will occur inevitably for the $NaREF_4$ nanocrystals beyond the critical size.

We also found that the spherical β-$NaEuF_4$ particles grew further anisotropically with increasing the concentration of $Na(CF_3COO)$, and their exposed facets changed. For example, with injecting 0.9 mmol $Na(CF_3COO)$ (dissolved in 1 mL of OA/ODE) into 19.1 nm-sized β-$NaEuF_4$ nanosphere solution, the

hexagonal nanospheres grew anisotropically. Figure 8g depicts the TEM image of the $NaEuF_4$ product obtained after 5 min with $Na(CF_3COO)$ injected, and it can be seen that the spherical particles were elongated slightly. Figure 8h reveals the HRTEM image combined with FFT analysis (inset) of one particle. Although the (20−20) and (11−20) facets can be seen, obviously different from the case of spherical particle (Figure 8f), the (0001) lattice fringes can be found perpendicular to the elongated direction of the particle. Moreover, for the particles with higher aspect ratio, the FFT pattern was quite different, and (0001) and (10−10) lattice fringes were found obviously (Figure S11g). With extending the reaction time for a further 5 min, uniform 24.6 nm × 35.7 nm nanorods were obtained, and the exposed facets of these rods were {0001} and {10−10} (Figure 3e). The rod-shape was thus considered thermodynamically stable, and the spherical shape might be controlled by kinetics.

Group III (Dy to Lu, Y). For group III, it was difficult for α-$NaREF_4$ to transform into β-$NaREF_4$ under mild conditions (Table S4). Figure 9 illustrates the α → β phase transition process of $NaYF_4$ with 1 mmol 12.2 nm α-$NaYF_4$ nanopolyhedra and 1 mmol $Na(CF_3COO)$ as the precursors reacted at 330 °C. After 5 min, the particles became nonuniform (Figure 9b), indicating that Ostwald-ripening occurred.[5] When the reaction was carried on further for 3 min, more β-$NaYF_4$ nanocrystals were formed (Figure 9a). From the TEM image we can see that a mixture containing a large portion of α-$NaYF_4$ nanopolyhedra in small sizes and some β-$NaYF_4$ hexagonal nanoplates in much larger sizes were obtained (Figure 9c). Moreover, it can be found that the edges of some hexagonal nanoplates were not straight, which were called the snowflake-shaped plates. With extending the reaction time to 12 min, the small particles were completely consumed, and the phase-pure β-$NaYF_4$ particles in large sizes were obtained, which contained a major potion of hexagonal plates and some snowflake-shaped plates (Figures 9a and S12). From the TEM and HRTEM images shown in Figure 9d, it could be seen that the direction of the tip of the snowflake was the {11−20} facets and that of the concave was the {10−10} facets. When the reaction was further extended to 15 min, no snowflake-shaped particles were found, and only large hexagonal plates with straight edges were obtained (Table S3).

As discussed above, the α → β phase transition process and the growth kinetics of β-$NaYF_4$ nanocrystals were some different from those of β-$NaEuF_4$ ones. The growth of β-$NaYF_4$ nanocrystals essentially required a high $Na(CF_3COO)$ concentration, and thus a more drastic process was dominant. In the early stage of this process, some nanopolyhedra were dissolved and became smaller, whereas some others grew larger (Figure 9b). During this period, no α → β phase transition occurred for $NaYF_4$ (Figure 9a). As concluded for $NaEuF_4$ above, the α → β phase transition should occur for larger $NaYF_4$ particles beyond the critical size. However, for $NaYF_4$, different from the case of $NaEuF_4$, large β-$NaYF_4$ hexagonal nanoplates and small α-$NaYF_4$ nanopolyhedra rather than the uniform nanocrystals coexisted at the mix-phase stage (Figure 9c). Then, the small α-$NaYF_4$ nanopolyhedra were dissolved, and the large β-$NaYF_4$ hexagonal nanoplates grew, showing {11−20} and {20−20} facets first. As the nanocrystal growth continued, the lattice fringe attributed to the low-index (10−10) plane was observed from the FFT pattern of the HRTEM image. Therefore, the particles became snowflake-shaped due to the variation of the relative growth rate of {11−20} to {10−10} facets. With extending the reaction time, the exposed {11−20} facets disappeared, and the edges of the hexagonal plates became straight. As a result, only {10−10} facets were exposed as the side faces of β-$NaYF_4$ hexagonal nanoplates. For β-$NaREF_4$ in group III, the hexagonal plate might be the thermodynamically stable shape, which was also obtained through the route using $Na(CF_3COO)$ and $RE(CF_3COO)_3$ as the precursors (Figure S13).

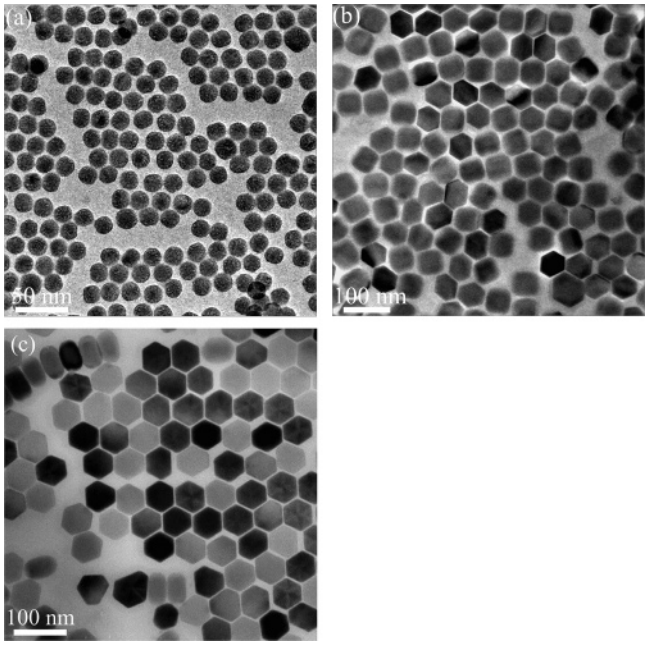

Figure 10. (a) TEM image of the $NaYF_4$ product obtained under 330 °C in OA/ODE (1:1) for 15 min (precursor: 1.8 mmol $Na(CF_3COO)$ and 1 mmol $Y(CF_3COO)_3$). TEM images of the $NaYF_4$ products obtained under 330 °C in OA/ODE (1:1) for (b) 25 min and (c) 45 min (precursor: 1.9 mmol $Na(CF_3COO)$ and 1 mmol $Y(CF_3COO)_3$).

In a brief summary, the rods and the hexagonal plates might be thermodynamically stable for β-$NaREF_4$ nanocrystals of group I (Pr and Nd) and group III (Dy to Lu,Y), respectively, and uniform β-$NaREF_4$ (RE = Pr and Nd) nanorods and β-$NaREF_4$ (RE = Dy to Lu, Y) nanoplates can be prepared both from the α-$NaREF_4$ precursor route and the $RE(CF_3COO)_3$ precursor route. For group II (Sm to Tb), β-$NaSmF_4$ and β-$NaEuF_4$ generally took the rod shape, whereas β-$NaGdF_4$ and β-$NaTbF_4$ may take the rod or plate shape, depending on the synthetic route (Tables S2 and S3). It should also be noted that, for β-$NaREF_4$ nanocrystals of group II, uniform rod- or plate-shaped ones can be obtained only through the α-$NaREF_4$ precursor route.

5. Shape-Control of β-$NaREF_4$ (RE = Y, Er) Nanocrystals. β-$NaYF_4$ and β-$NaErF_4$ nanocrystals with different shapes can be selectively synthesized by tuning the ratio of Na/RE using $Na(CF_3COO)$ and $RE(CF_3COO)_3$ as the precursors. Taking β-$NaYF_4$ as an example, when the ratios of Na/Y were 1.8, 1.9 and 2.1, 26.6 nm × 47.6 nm nanorods (aspect ratio = 1.8), 58.9 nm × 52.6 nm hexagonal nanoplates (aspect ratio = 0.90) and 155 nm × 76 nm hexagonal nanoplates (aspect ratio = 0.49) were obtained, respectively (Figures 3a, 10b, and 3c). With the low ratio of Na/Y, β-$NaYF_4$ nanocrystals tended to grow as rods. When the reaction time was shortened to 15 min, uniform hexagonal nanospheres were obtained (Figure 10a), indicating that the β-$NaYF_4$ rods were formed through the anisotropical growth of the spherical particles, just like the growth

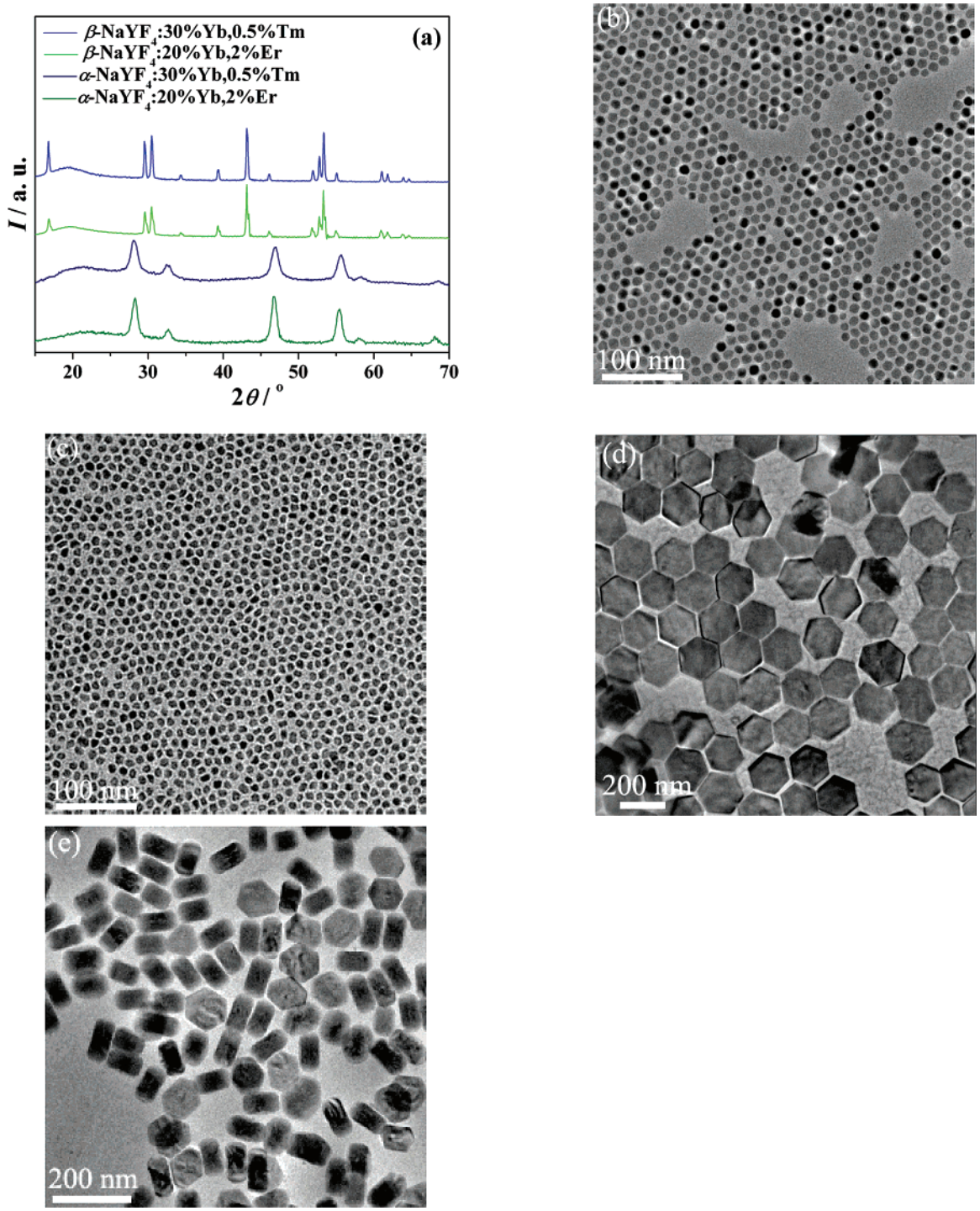

Figure 11. (a) XRD patterns of α-$NaY_{0.78}Yb_{0.2}Er_{0.02}F_4$, β-$NaY_{0.78}Yb_{0.2}Er_{0.02}F_4$, α-$NaY_{0.695}Yb_{0.3}Tm_{0.005}F_4$, and β-$NaY_{0.695}Yb_{0.3}Tm_{0.005}F_4$ nanocrystals. TEM images of α-$NaY_{0.78}Yb_{0.2}Er_{0.02}F_4$ nanopolyhedra (b), α-$NaY_{0.695}Yb_{0.3}Tm_{0.005}F_4$ nanopolyhedra (c), β-$NaY_{0.78}Yb_{0.2}Er_{0.02}F_4$ hexagonal plates (d), and β-$NaY_{0.695}Yb_{0.3}Tm_{0.005}F_4$ hexagonal plates (e).

of β-$NaEuF_4$ rods. However, when increasing the ratio of Na/Y (Na/Y = 1.9), the growth rate of β-$NaYF_4$ nanocrystals along *a*-axis was markedly quickened, and the aspect ratio decreased with extending the reaction time (Figure 10c). The shape-controlled synthesis of β-$NaErF_4$ nanocrystals is similar to that of β-$NaErF_4$ ones, and the results are shown in Figure S14.

6. Synthesis of High-Quality $NaYF_4$:Yb,Er/Tm Nanocrystals. On the basis of the above study on the controlled synthesis of single rare-earth $NaREF_4$ nanocrystals, we also prepared high-quality $NaYF_4$:Yb,Er/Tm nanocrystals by co-decomposition of $Na(CF_3COO)$, $Y(CF_3COO)_3$, $Yb(CF_3COO)_3$, and $Er(CF_3COO)_3$/$Tm(CF_3COO)_3$ in OA/OM/ODE. The XRD pattern indicates that pure cubic and hexagonal $NaYF_4$:Yb,Er/Tm were obtained (Figure 11a). TEM characterization has revealed that α-$NaY_{0.78}Yb_{0.2}Er_{0.02}F_4$ and α-$NaY_{0.695}Yb_{0.3}Tm_{0.005}F_4$ nanocrystals are of polyhedron shape with the size of 13.6 and 10.8 nm, respectively (Figure 11b,c). The β-$NaY_{0.78}Yb_{0.2}Er_{0.02}F_4$ and β-$NaY_{0.695}Yb_{0.3}Tm_{0.005}F_4$ nanocrystals are hexagonal plates with the size of 187 nm × 71 nm and 100 nm × 51 nm, respectively (Figure 11d,e).

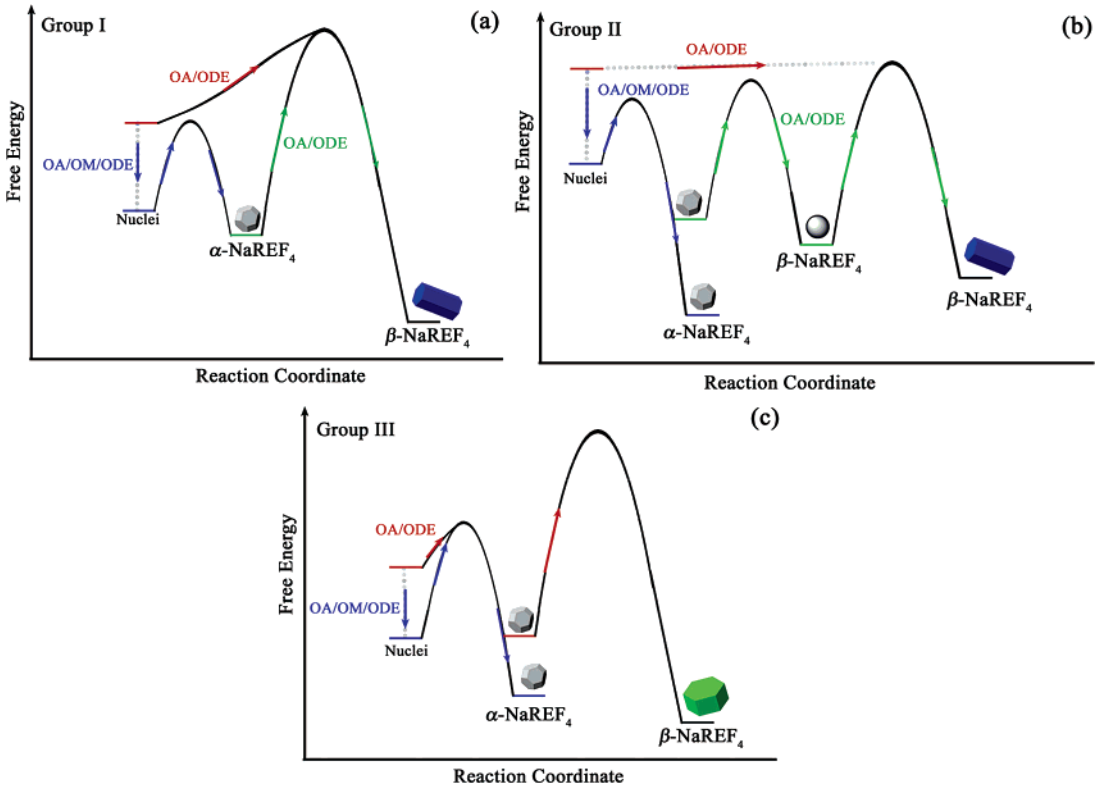

Figure 12. Schematic illustration of the free energy for the controlled synthesis of $NaREF_4$ nanocrystals (I: Pr and Nd; II: Sm to Tb; III: Dy to Lu, Y).

7. Free Energy Schemes for the Controlled Synthesis of $NaREF_4$ Nanocrystals. The controlled synthesis of $NaREF_4$ nanocrystals in the present work could be explained from the point of view of system-free energy without considering the free energy change of organic species.[3b,4e] According to the different growth behavior of $NaREF_4$ nanocrystals, the free energy scheme is simply depicted in Figure 12.

For group I in OA/ODE, β-$NaREF_4$ (RE = Pr and Nd) hexagonal nanorods were formed directly from REF_3, for α-$NaREF_4$ was not so stable as REF_3 (Figure 12a, the path marked in red). In addition, when using α-$NaREF_4$ nanopolyhedra and $Na(CF_3COO)$ as the precursors, the proper energy barrier for the nanocrystal growth also led to the formation of the thermodynamically stable nanorods in OA/ODE, (Figure 12a, the path marked in green). For group II, β-$NaREF_4$ (RE = Sm to Tb) nanocrystals were formed directly in OA/ODE (Figure 12b, the path marked in red). As the energy barrier was considered to be relatively low, the growth of β-$NaREF_4$ should be so fast that only irregular particles were obtained. Also for group II, the free energy of α-$NaREF_4$ nanopolyhedra is considerably lower than that of the $NaREF_4$ nuclei, so the increased energy barrier has greatly retarded the growth of the nanocrystals. Under this condition, using α-$NaREF_4$ nanopolyhedra and $Na(CF_3COO)$ as the precursors results in uniform β-$NaREF_4$ nanospheres and nanorods in turn with extending the reaction time in OA/ODE (Figure 12b, the path marked in green). For group III, the energy barrier to the formation of β-$NaREF_4$ (RE = Dy to Lu, Y) is so high that α-$NaREF_4$ is stable even in OA/ODE. Only under the drastic conditions, were the thermodynamically stable β-$NaREF_4$ hexagonal plates obtained (Figure 12c, the path marked in red). The addition of OM makes α-$NaREF_4$ in the three groups more stable, and the energy barrier between α-$NaREF_4$ and β-$NaREF_4$ is increased. Therefore, uniform α-$NaREF_4$ nanopolyhedra were obtained, and were hardly transformed into β-$NaREF_4$ nanorods or hexagonal plates (Figure 12, the path marked in blue).

8. Photoluminescent Properties of $NaEuF_4$ Nanocrystals. To study the photoluminescent properties of α-$NaEuF_4$ and β-$NaEuF_4$ nanocrystals, high-quality 5.0 ± 0.4 nm, 6.3 ± 0.5 nm, and 8.1 ± 0.5 nm α-$NaEuF_4$ nanopolyhedra (Figures S9c, 2b, and 8a); 19.1 ± 0.9 nm β-$NaEuF_4$ nanospheres (Figure 8e), and (24.6 ± 1.6) nm $\times$ (35.7 ± 1.5) nm β-$NaEuF_4$ nanorods (Figure 3e) were prepared. Figure 13a shows the room-temperature emission spectra of the as-obtained α-$NaEuF_4$ nanopolyhedra redispersed in toluene/hexane (1:1). The spectra are characteristic of the $^5D_0 \rightarrow {}^7F_j$ line emissions ($J = 0$, 1, 2, 3, 4) of the Eu^{3+} ion. Interestingly, the $^5D_0 \rightarrow {}^7F_2$ transition became stronger with decreasing the crystallite size, and the ratio of I_{610}/I_{590} is 1.5, 2.3, and 3.0 for 8.1, 6.3, and 5.0 nm α-$NaEuF_4$ nanopolyhedra, respectively. It is well-known that the $^5D_0 \rightarrow {}^7F_2$ transition is electric-dipole transition, and its intensity is significantly affected by the symmetry in local environments around Eu^{3+} ions.[17,18] When the symmetry around the Eu^{3+} ions is lowered, the transition probability of the $^5D_0 \rightarrow {}^7F_2$ is increased. However, the $^5D_0 \rightarrow {}^7F_1$ transition is magnetic-dipole allowed and is relatively insensitive to the local symmetry.[17b,18] As for the surface atoms with a lower coordination number, they usually have lower symmetry than the bulk ones. Thus, when the size of the α-$NaEuF_4$ nanocrystals decreased, the ratio of surface Eu atoms increased; as a result, the value of I_{610}/I_{590} increased.

(17) (a) Zakaria, D.; Mahiou, R.; Avignant, D.; Zahir, M. *J. Alloy Compd.* **1997**, *257*, 65. (b) Wang, F.; Fan, X. P.; Pi, D. B.; Wang, M. Q. *Solid State Commun.* **2005**, *133*, 775. (c) Wei, Z. G.; Sun, L. D.; Jiang, X. C.; Liao, C. S.; Yan, C. H.; Tao, Y.; Zhang, J.; Hu, T. D.; Xie, Y. N. *Chem. Mater.* **2003**, *15*, 3011.
(18) Judd, B. R. *Phys. Rev.* **1962**, *127*, 750.

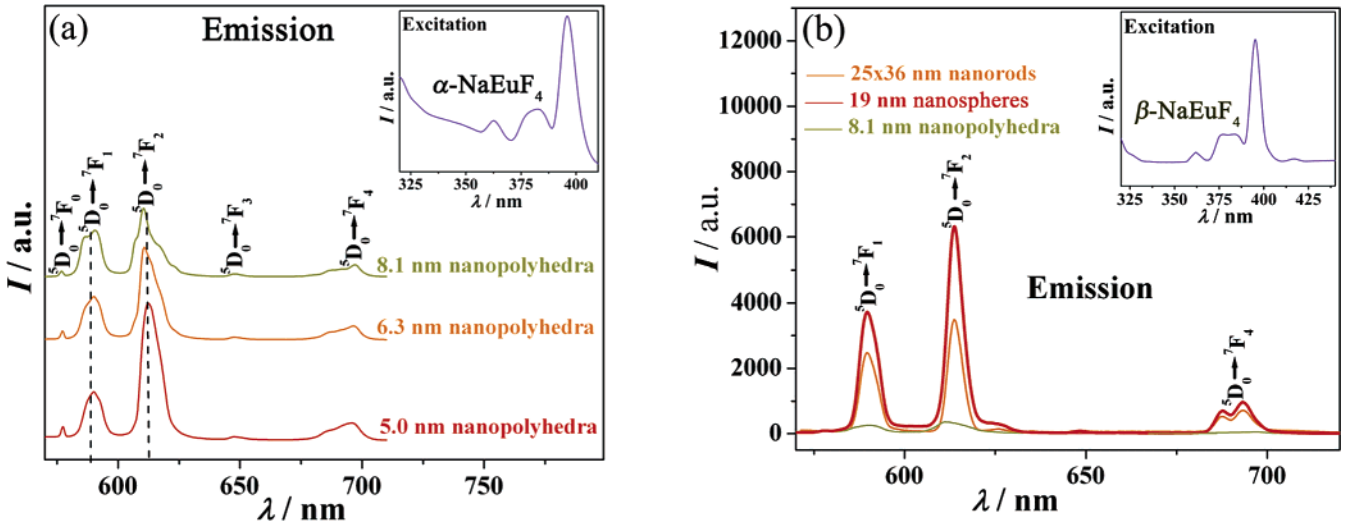

Figure 13. Room-temperature fluorescence emission spectra of α-$NaEuF_4$ nanopolyhedra with different sizes (λ_{ex} = 396 nm) (a), and of α-$NaEuF_4$ nanopolyhedra, β-$NaEuF_4$ nanospheres, and β-$NaEuF_4$ nanorods (b) dispersed in hexane/toluene (1:1) under 0.1 mol L^{-1}; insets are their excitation spectra (λ_{em} = 610 nm).

Figure 13b displays the emission spectra of α-$NaEuF_4$ and β-$NaEuF_4$ nanocrystals. The emission intensity of the β-$NaEuF_4$ nanospheres and nanorods was more than 10 times as high as that of the α-$NaEuF_4$ nanopolyhedra, due to the more ordered structure of β-$NaEuF_4$,[15] along with their larger sizes. It was also noted that the emission intensity of β-$NaEuF_4$ nanospheres was 1.5 times as high as that of the β-$NaEuF_4$ nanorods. As it is well-known that the lower the symmetry is around the emitting ion, the stronger is the emission in lattices.[17a] The symmetry of all Eu^{3+} ions in the 19.1 nm β-$NaEuF_4$ nanospheres was lower than that in the β-$NaEuF_4$ rods because of the higher surface atom fraction of nanospheres. As a result, the emission intensity of the nanospheres was higher than that of the nanorods. For bulk β-$NaEuF_4$,[17a] I_{610}/I_{590} is less than 1. In contrast, the value of I_{610}/I_{590} for our β-$NaEuF_4$ nanorods and nanospheres increased up to 1.2 and 1.6, respectively, also because of the increasing fraction of the surface Eu atoms for our $NaEuF_4$ nanocrystals. Although the ratio of surface Eu atoms in 19.1 nm β-$NaEuF_4$ nanospheres was lower than that in 8.1 nm α-$NaEuF_4$ nanopolyhedra, the whole symmetry of Eu^{3+} in β-$NaEuF_4$ was lower. Consequently, the value of I_{610}/I_{590} of the 19.1 nm β-$NaEuF_4$ nanospheres was higher than that of the 8.1 nm α-$NaEuF_4$ nanopolyhedra.

Conclusions

We have demonstrated a general synthesis of high-quality α- and β-phase $NaREF_4$ and $NaYF_4$:Yb,Er/Tm nanocrystals through the co-thermolysis of $Na(CF_3COO)$ and $RE(CF_3COO)_3$ in oleic acid/oleyamine/1-octadecene, which has the merits of one-step, mass production, and easy operation. By tuning the ratio of Na/RE, solvent composition, reaction temperature, and time, we can manipulate the phase, shape, and size of the $NaREF_4$ nanocrystals. The principles of the α → β phase transition and shape-selective synthesis of our $NaREF_4$ nanocrystals have been revealed through carefully controlling their growth kinetics. It is confirmed that the α → β phase transition is closely correlative with the particle size, and the shape-selective synthesis can be carried out by controlling the thermodynamic or kinetic growth of the nanocrystals. These results not only enrich the contents of lanthanide and fluoride chemistry but also contribute to the principles of the crystal growth and phase transition of inorganic materials. In addition, the size- and shape-dependent photoluminescent properties can be observed in the high-quality $NaEuF_4$ nanocrystals. For the future, we believe that the developed route via the thermolysis of metal trifluoroacetates in high-boiling solvents may be further generalized to synthesize other pure or doped complex fluoride nanocrystals (e.g., $LiREF_4$ and $KREF_4$; see Figure S15; $M_xM'_yF_z$, M = alkali or alkaline-earth metal, M′ = rare-earth or transition metal). Our further studies are currently underway to deeply investigate the optical properties of $NaREF_4$ nanocrystals and to extend the present synthetic route to more complex metal fluoride nanocrystals.

Acknowledgment. We gratefully acknowledge the financial aid from the MOST of China (Grant No. 2006CB601104) and the NSFC (Grant Nos. 20571003, 20221101, and 20423005).

Supporting Information Available: Summary of the synthetic conditions and the characteristics of the products (Tables S1−S4), more XRD and TEM results for $MREF_4$ (M = Na, K, Li) nanocrystals, ^1H NMR spectrum of the α-$NaYF_4$ product in $CDCl_3$, EDAX spectrum of the α-$NaYF_4$ product, and size distribution histograms of $NaYF_4$ nanocrystals. This material is available free of charge via the Internet at http://pubs.acs.org.

JA060212H